Global hyper-resolution groundwater dataset for assessing historical and future groundwater dynamics

Barry van Jaarsveld[1], Niko Wanders[1], Nicole Gyakowah Otoo[1], Edwin H. Sutanudjaja[1], Jarno Verkaik[2], Daniel Zamrsky[1], and Marc F.P. Bierkens[1,2]

[1]Utrecht University, Department of Physical Geography, Princeton laan 8a, Utrecht, The Netherlands

[2]Deltares, Unit Subsurface and Groundwater Systems, Utrecht, The Netherlands

Correspondence: Barry van Jaarsveld (a.s.vanjaarsveld@uu.nl)

Abstract

Sustainable management of global groundwater is a key societal challenge and central to Sustainable Development Goals. To address limited observations and coarse global models, we present a global hyper-resolution dataset of monthly groundwater heads and water table depth at 30 arc-seconds (~1 km), simulated by GLOBGM, a global groundwater flow model. The data set follows ISIMIP protocols and enables comparison of impacts of climate change between sectors and models. Using ISIMIP3a inputs, groundwater dynamics is simulated for a reference period (1960–2019) to support model evaluation and attribution of observed impacts to climate variability and change. Following ISIMIP3b, historical baselines (1960–2014) and three combined socioeconomic–climate scenarios (2015–2100; SSP1-RCP2.6, SSP3-RCP7.0, SSP5-RCP8.5) are simulated with five GCMs, supporting robust detection and impact assessment of future change. Regions of reduced reliability are mapped and quality assurance flags are provided to guide appropriate use and interpretation. The dataset offers comprehensive, high resolution information to assess groundwater dynamics for past and future, supporting improved global water resource management and climate impact assessments.

Background & Summary

Groundwater is the most abundant source of fresh liquid water; globally, 98% of accessible fresh liquid water is in the form of groundwater[1,2]. Since the advent of mechanical drilling, people have relied on groundwater resources to supplement available surface water supplies to meet total water demands[3]. As a result of a growing population and associated increases in water demand for agriculture, domestic and industrial purposes, the (unsustainable) use of groundwater has increased significantly in the past decades[1,4–9]. Groundwater is vulnerable to overexploitation when abstraction rates exceed rates of recharge; which has been shown to cause a decline in groundwater storage in many regions of the world[9,10]. In addition to anthropogenic impacts, groundwater dynamics is also sensitive to climate variability and its affects on groundwater recharge; which are complex and vary geographically[11,12]. The extent to which recharge variations affect groundwater is determined by the interaction between topography, vegetation characteristics, underlying geological properties, and the connectivity between surface water and groundwater[12,13]. For example, groundwater in deep confined aquifers with low permeability is relatively insensitive to changes in recharge, while groundwater in highly permeable shallow aquifers with vegetation characteristics that facilitate exchanges across the land-atmosphere continuum are more closely coupled to recharge dynamics[13–15]. Therefore, the dynamics of groundwater reserves has been and will continue to be driven by complex interactions between society, climate, and ecosystems[6,16].

Overexploitation of groundwater can cause the depths of the water table to deepen, which is evident throughout the world and especially in regions with little or no surface water supply, such as arid and dry land regions[17,18]. Physical and economic constraints mean that deeper groundwater becomes a less reliable water source[19]. Given that over half of global river flows are groundwater sustained, the deepening of water table depths also poses a threat to future surface water supplies[20–22], which may increase vulnerability to hydrological drought[4]. In addition to the negative effects related to water supply, reduced groundwater reserves have been shown to aggravate the negative impacts of land subsidence, rising sea level, and impact groundwater quality[4,7]. Deeper water table depths also influence the composition and functioning of groundwater-dependent ecosystems and the ecosystem services they provide[23–25]. Ultimately, groundwater forms an important component of global socio-ecological systems and the earth system as a whole[26].

Sustainable management of the world's remaining groundwater reserves is a key societal challenge and is cited in a number of sustainable development goals[27,28]. Policy makers must develop and implement adaptation and mitigation strategies that secure groundwater availability to ensure groundwater levels are kept within safe operating limits for society. To achieve this goal, we need to ensure that reliable estimates of current and future groundwater volumes are available. Relying solely on observational groundwater data to estimate current groundwater volumes is insufficient given the severe limitation in the availability of globally uniform data in terms of spatial and temporal coverage[28,29]. For example, the current state-of-the-art datasets contains data 180,000 time series from 41 countries of which over 90% of these time series occurring in North America, Australia, or Europe[30]. To overcome this challenge and provide global-scale information, water managers rely on physically-based numerical global groundwater models[29]. However, to date, most groundwater flow models have limited spatial extent that allows for, at most, regional-scale assessments (1,000,000 km^2)[31]. Only recently have groundwater models with global extent been formulated[32–35], of which only two models support transient simulations. However, global groundwater models provide information at spatial resolutions that are often too coarse to meet the demands of policy makers and stakeholders, who require more fine-scale information[29,36]. To overcome this limitation, we need to further enhance the spatial resolution of these models to make them more locally relevant and actionable[36,37].

To this end, hyper-resolution groundwater models have been highlighted for their potential to include climate, vegetation, and anthropogenic influences on groundwater at appropriate spatial resolutions for the past and a climate change-affected future[36]. This is especially relevant given that climate change has been identified as an important driver of current water scarcity hotspots[9]. Recent work has shown that applying global groundwater models at the ~1 km spatial resolution is possible with today's high-performance computers[38]. This technical milestone thus provides the opportunity for global hyper-resolution estimates of past and future groundwater reserves. The objective of this study is: to provide the first hyper-resolution monthly estimates of groundwater reserves for the past and a climate change informed future. To this end, we use a global hyper-resolution model (30 arc-seconds, ~1 km at the equator) that simulates monthly groundwater heads and water table depths. This dataset is developed using the framework and protocols of the Inter-Sectoral Impact Model Intercomparison Project (ISIMIP), thus providing a standardized basis for comparing climate change impacts across different sectors and models[39]. Using the ISIMIP3a protocol and associated inputs to provide

estimates of groundwater reserves for the historic period (1960 - 2019), which can be used for the detection and attribution of past climate change and socioeconomic impacts on groundwater reserves. In addition, the ISIMIP3b protocol is used to provide global groundwater estimates for the historical baseline (1960 - 2014) and future projections (2015 - 2100) under combined socio-economic and climate scenarios SSP1-RCP2.6, SSP3-RCP7.0, and SSP5RCP8.5 - using a suite of five Global Climate Models (GCMs) to allow for uncertainty quantifications due to climate variability.

Since the data produced here were generated following the ISIMIP framework, the data here are intended for use following this framework. More specifically, the historical reference simulation (ISIMIP3a) can be used for model evaluation against observed data, as is done in this work, and for studies concerned with multi-model uncertainty[40]. Simulations following the ISIMIP3b framework can be used to support studies that investigate climate change related risks on global groundwater reserves. As stated in the proposed ISIMIP groundwater sector framework, groundwater heads and water table depths data will facilitate cross-sectoral research such as the impact of changing groundwater reserves on social, economic, and ecological systems - such as health impacts, water quantity and quality, land cover change, and even fires[41].

Users are especially encouraged to leverage existing earth system data sets to relate groundwater dynamics to other earth system components[42]. In addition to the advantages provided by the high spatial and temporal resolution estimates of groundwater reserves presented here, the inclusion of multiple climate models in three combined climate and socioeconomic climate projections allows the incorporation of uncertainty and enhances the robustness of the results derived from future studies. For example, water table depth is a critical parameter when assessing the ecological impacts of groundwater depletion[25]. By analyzing these impacts using multiple models, it becomes possible to quantify uncertainty and improve confidence in projections. Ultimately, the data presented here serve as a baseline for future studies aimed at exploring the role of adaptation and mitigation strategies involving groundwater.

Methods

The methods section is structured as follows. First, an overview of the model used in this study, GLOBGM, is provided, with additional reference to any changes that were made compared to the original publication (GLOBGMv1.0)[38]. Thereafter, we present the methodology associated

with model calibration and the derivation of initial states. This is followed by information pertaining to the simulations.

The GLOBGM v1.1 model

Monthly estimates of groundwater heads and water table depths presented here were simulated using GLOBGM[38], a 30 arc-seconds global two-layer transient MODFLOW-based groundwater model and the successor to the 5 arc-minute global groundwater model[35]. GLOBGM is based on a prototype version of MODFLOW6, which is parallelised using a message-passing interface and makes use of unstructured grids. Independent unstructured grids are distributed over three continental-scale groundwater models - Afro-Eurasia, America, Australia - and one remaining model for the islands (Figure 1). Each of the four groundwater models is partitioned into non-overlapping sub models that are coupled within the MODFLOW linear solver. GLOBGM is a two-layer groundwater model that is used to represent unconfined or confining and confined aquifers[38]. For cells where a confining layer is present, the top model layer represents this confining layer and the bottom layer is the confined aquifer; in regions where a confining layer is absent, the bottom model layer represents the unconfined aquifer. GLOBGM employs an offline coupling approach whereby local runoff, groundwater abstraction, and groundwater recharge outputs, at the 5 arc-minutes resolution, are derived from PCR-GLOBWB2 and used as inputs to simulate groundwater dynamics[43]. GLOBGM can be used to simulate groundwater heads and water table depths using either a steady state solution or a transient solution. The steady state solution is used to estimate average groundwater patterns under stable or long term average conditions and abstraction is not considered. The transient solution allows for the modelling of groundwater patterns over time and incorporates abstraction. For brevity, we refer the reader to the original publication for a more detailed description of model inputs, parametrization, and runtime configurations; in the text that follows, we describe any changes made that deviate from the original version[38].

Given that GLOBGM employs an offline coupling approach whereby 5 arc-minute local runoff, groundwater abstraction, and groundwater recharge from PCR-GLOBWB2 are provided as input to the model, a form of resampling or downscaling is required to match the 5 arc-minutes input with the 30 arc-seconds grid of GLOBGM. GLOBGMv1.0 made use of the nearest neighbour resampling algorithm to re-grid the 5 arc-minutes recharge and abstraction to 30 arc-seconds resolution[38]. However, local runoff was converted to surface water discharge by accumulating it through the 30 arc-seconds river drainage network of

HydroSHEDS[44]. In the simulations we present here, the treatment of groundwater abstraction and local runoff remains unchanged. However, we do introduce a method to correct and downscale groundwater recharge based on observational records and implement a dynamic drainage elevation using saturated area fraction. Implementing a dynamic drainage elevation

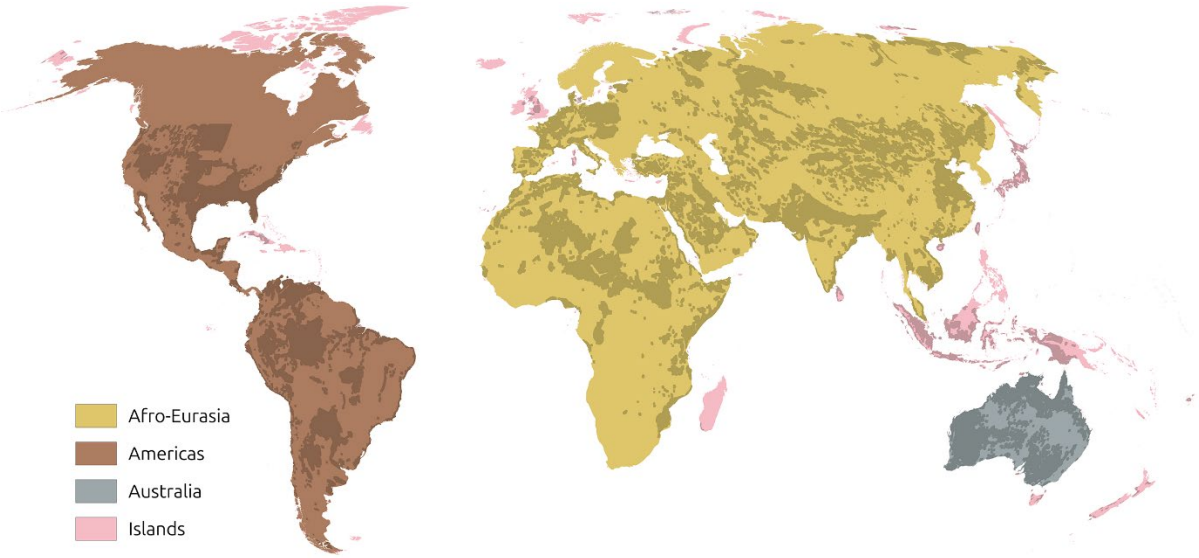

Figure 1. The four groundwater models that constitute GLOBGM - a global groundwater model. Dark overlays indicate the presence of a confining layer.

based on the saturated area fraction enables a better representation of more permanent wetland areas, maintaining groundwater levels closer to the surface, and reducing the occurrences of highly intermittent groundwater discharge and fluctuations in groundwater levels.

Groundwater Recharge Correction

Groundwater recharge is notoriously difficult to accurately predict using current global hydrological models[4,40,45]. Previous studies have shown that the recharge rates predicted by PCRGLOBWB2, to which GLOBGM is coupled, are on average underestimated compared to observed data, especially in arid or semi-arid regions where recharge is relatively low, intermittent and unpredictable[46]. Taking this into account, and considering that GLOBGMv1.0 has been shown to predict groundwater heads that are, broadly speaking, lower than in situ observations and other large-scale groundwater models[38,40] - for this study groundwater recharge rates supplied to GLOBGMv1.1 were corrected based on observed groundwater recharge rates. A Generalized Additive Model regression approach, using pyGam[47], was used to create a long term averaged groundwater recharge field ($GWR_{observed}$) from observations and high resolution data of known drivers and covariates of groundwater recharge (Table 1). This approach was previously used in the broader context of groundwater modelling context[31,48]. In

contrast to previous studies, land cover was not explicitly included as a predictor variable. Instead, groundwater recharge from PCR-GLOBWB2 was included as a predictor to capture residuals associated with land cover by proxy. To avoid cases where groundwater recharge exceeds precipitation, the corrected recharge product was post-processed so that the corrected long-term average groundwater recharge could not exceed the long-term average local precipitation[49,50].

Table 1. The response and predictor variables, and associated units, spatial resolution, and references used to calculate long term averaged groundwater recharge rates used as part of the groundwater recharge downscaling procedure.

Variable	Units	Spatial Resolution	Reference
Response			
Observed Groundwater Recharge	$m.year^{-1}$	30 arc-seconds	[12,51]
Predictors			
Aridity Index	-	30 arc-seconds	[52]
Clay Fraction, Sand Fraction, Silt Fraction	%	30 arc-seconds	[53]
Potential Reference Evaporation Precipitation	$m.year^{-1}$	30 arc-seconds	[49,50]
Recession Coefficient Slope Elevation Hydraulic conductivity	- - amsl $m.day^{-1}$	30 arc-seconds	[38]
PCR-GLOBWB2 recharge	$m.year^{-1}$	5 arc-minutes	[43,54]

For the steady-state simulation, $GWR_{corrected}$ was used as the recharge input. For the transient solution, $GWR_{observed}$ was compared to the long-term average 5 arc-minute groundwater recharge ($GWR_{5arc'}$) of PCR-GLOBWB2 to calculate a correction factor (GWR_{cf}, Equation 1). Then for each time step, the 5 arc-minute groundwater recharge from PCR-GLOBWB2 was interpolated to the 30 arc-seconds GLOBGMv1.1 grid using a bicubic interpolation algorithm and bias corrected ($GWR_{corrected}$) using GWR_{cf} (Equation 2). However, the monthly $GWR_{corrected}$ fields, without further processing, would lead to unrealistically high values, particularly for months when PCR-GLOBWB2 shows zero recharge or when monthly recharge rates exceed the long-term averages. Therefore, the bias-corrected recharge rates ($GWR_{corrected}$) were constrained so that it did not exceed the 5 arc-minute precipitation for that month (P_{month}; Equation 3).

$$GWR_{cf} = \frac{GWR_{observed}}{GWR_{5arc'}} \quad (1)$$

$$GWR_{corrected} = GWR_{5arc'} \times GWR_{cf} \quad (2)$$

$$GWR = \begin{cases} P_{month}, & GWR_{corrected} < P_{month} \\ GWR_{corrected}, & GWR_{corrected} \leq P_{month} \end{cases} \quad (3)$$

Saturated Area Fraction

To simulate variations in the saturated area fraction, we use the improved ARNO scheme[55,56], which is an integral part of PCR-GLOBWB2, to assess the area subject to surface runoff. In this version of GLOBGMv1.1, the drain elevation is dynamically adjusted according to soil saturation (Equation 4). As the soils become wetter, the model lifts the drainage elevation closer to the surface; as they dry, it drops it back to the base. Discharge only occurs when the groundwater head rises above the dynamic drain level. Adjusting the drain elevation with saturated area fractions allows the simulation of more permanent wetland areas with groundwater levels closer to the surface and preventing strongly intermittent groundwater discharge and groundwater levels.

$$satAreaFrac = \left(\frac{W_{max} - S_{tot}}{W_{max} - W_{min}}\right)^{\frac{\beta}{\beta+1}} \quad (4)$$

Where W_{max} is the maximum water storage, W_{min} is the minimum water storage, W_{max} is the total water storage, β is the ARNO beta.

Calibration and initial conditions estimation

The previous GLOBGMv1.0 model was uncalibrated and established its initial groundwater conditions using a method inherited from its predecessor, PCR-GLOBWB2[35,38]. This process involved simulating groundwater heads under natural conditions with a steady-state solution and then using those estimates as a starting point for a transient spin-up period to reach equilibrium. However, this approach is subject to improvement, given that uncalibrated models have been shown to be less accurate than their calibrated counterparts, such as the CONUS groundwater model and the global-scale inverse model[24,38,57], and that spurious spin-up trends are evident in model output. To address these limitations, the simulations presented here use a calibrated version of GLOBGM and an alternative spin-up procedure is implemented to provide more reliable initial states and eliminate the spurious trends found in GLOBGMv1.0[38].

Calibration

In an effort to improve the model's accuracy in simulating groundwater heads and water table depths, we calibrated hydraulic conductivity, anisotropy and entrance resistance parameters using the steady-state solution. To calibrate anisotropy and entrance resistance parameters, a range of global prefactor adjustments were assessed (Table 2). A broader range of calibration prefactors could have been considered; however, given that the observations non uniformly distributed and to avoid significant departures the original model parametrisation, the selected parameter ranges were limited to within two orders of magnitude. Calibrations on the 5 arc-minute predecessor to GLOBGM have shown a limited model sensitivity to variations in hydraulic conductivity when a global prefactor is applied to the entire model domain[25]. Therefore, to introduce regional sensitivities to changes in hydraulic conductivity, we assessed different combinations of prefactors (Table 2) that varied according to lithological class as defined in the GLiM dataset[58]. In total, 162 permutations were assessed.

Table 2. Table showing the parameters subject to calibration and the candidate values for each. Lithology class was obtained from the GLiM data set[58].

Variable	Lithology	Candidate values
Ks	Fine + coarse unconsolidated	0.1 - 1.0 - 10.0
	Fine + coarse	0.1 - 1.0 - 10.0
	Carbonate	0.1 - 1.0 - 10.0
Anisotropy	Consistent across lithologies	0.1 - 1.0
Entrance resistance	Consistent across lithologies	0.1 - 1.0 - 10.0

The steady-state solution was forced using historical reference data, but used PCR-GLOBWB2 outputs from a natural run under pristine natural conditions (i.e., no anthropogenic influence). It is important to note that we included updates to the model regarding groundwater recharge downscaling and saturated area fraction adjustments prior to calibration. To choose the best set of calibration settings, we relied on long-term averaged observed groundwater table depths that overlapped with the time period of the forcing data (i.e., 1960-2019). Observed groundwater table depth data were obtained from IGRAC's Global Groundwater Monitoring Network[59]. Given that the steady-state solution of GLOBGMv1.1 was forced with data representative of the earth's hydrological cycle in a pristine state (i.e., unaltered by anthropogenic influence on surface water and groundwater dynamics), we set out to create a set of observed data that excluded regions where anthropogenic modification to the hydrological cycle is known to have occurred. Therefore, the observed data were filtered to exclude any known hotspots for water scarcity[9], as they are likely influenced by extensive pumping. From this filtered dataset of

34,800 observation wells, we evaluated each calibration permutation by calculating the bias (WTD_{bias}; Equation 5) over all observation wells as the objective function.

$$WTD_{bias} = WTD_{obs} - WTD_{sim} \quad (5)$$

Where WTD_{sim} is simulated water table depths, and WTD_{obs} is the observed water table depths.

To allow for a direct comparison between the model simulations and observations, we used the water table depth output provided by GLOBGMv1.1 which is converted from simulated groundwater heads using the surface elevation. Please note that due to this conversion and Equation 5, positive bias in this context means that simulated water table depths are shallower than observed; whereas negative bias is indicative of simulated water table depths being deeper than observed. For unconfined aquifers, where no confining layer is present, observations were assigned to the bottom layer of the model. In cases where a confining layer was present in the model, observations were assigned to the correct model layer based on the reported filter when present. If filter depth was not reported, the correct model layer was assigned through an approach that evaluates the correlation of remotely sensed soil moisture data with simulated groundwater heads – an approach for the validation of GLOBGMv1.0[38]. More specifically, if the observed water table depth displayed a correlation with soil moisture, the observation was assigned to the upper model layer (i.e., confining aquifer); whereas if no correlation is found, the observation is assigned to the bottom model layer (i.e., confined aquifer).

Initial conditions estimation

We set out to derive a set of initial states for groundwater heads for the starting year for the simulations presented here (i.e., 1960). In short, the goal of this approach is to obtain a set of starting points that resemble the observed data as closely as possible. As a first step, the steady-state estimates of groundwater head are estimated under pristine natural conditions, without anthropogenic influence. The steady-state result is then used as a starting point for a transient simulation for the year 1960, excluding pumping, which was run back-to-back for 75 iterations (i.e., years) in an attempt to achieve a dynamic steady state. Thereafter, a follow-on transient simulation, but with pumping activated, is run back-to-back for 50 iterations so that water table depths approach that of the observed levels for 1960. For this step, GLOBGMv1.1 was forced with data relevant to the historical reference simulation. As for the calibration step above, observed water table depth data were obtained from the IGRAC's Global Groundwater Monitoring Network and filtered data for the year 1960, which in total was 2,175 observation

wells. To determine each iteration's bias compared to simulated water table depth, WTD_{bias} (Equation 5) and relative mean absolute bias ($WTD_{relbias}$; Equation 6) were calculated.

$$WTD_{relbias} = \frac{WTD_{sim} - WTD_{obs}}{WTD_{obs}} \quad (6)$$

Where WTD_{sim} simulated water table depths, and WTD_{obs} the observed water table depths.

Note that a positive relative bias in this context means that simulated water table depths are shallower than observed; whereas a negative bias is indicative of simulated water table depths being deeper than observed. Simulated and observed water table depths were assigned to the correct model layer. The objective function for assessing the change in WTD_{bias} and $WTD_{relbias}$ over iterations was to converge on the smallest differences between the modelled and observed groundwater depths. In addition, to assess the evolution of head estimates over the model domain as a whole, the average groundwater head for each sub-model was calculated (HDS; Equation 7). The groundwater heads estimated at the final iteration were then used as the initial conditions for all subsequent simulations presented here.

$$HDS = \frac{1}{n \times m} \sum_{i=1}^{n} \sum_{j=1}^{m} h_{i,j} \quad (7)$$

Where h_{ij} is the groundwater head at a grid cell in row i in column j, n and m are the number of rows and columns, respectively.

Simulations

The updated and calibrated setup of GLOBGMv1.1 described in the preceding sections was used to produce global 30 arc-seconds estimates of groundwater heads and water table depth for a model evaluation and detection and attribution protocol[60], as well as future projections following the ISIMIP3b scenario-based simulation framework[60]. Given that GLOBGM requires 5 arc-minute PCR-GLOBWB2 outputs as forcing data through offline coupling, forcing data were obtained from the previously published PCR-GLOBWB2-based hydrological projection of future global water states with CMIP6 (HYPFLOWSCI6) dataset[54,61]. For the historical reference simulation (ISMIP3a), we used HYPFLOWSCI6 relevant to the GSWP3-W5E5 simulations for the period 1960 - 2019[54,61,62]. For the future projections, we have the historical baseline simulation (1960 - 2014) and the future (2015 - 2100) under an optimistic SSP1-RCP2.6, business-as-usual SSP3-RCP7.0, and pessimistic SSP5- RCP8.5 scenarios for 5 Global Circulation Models (GMCs). The following GCMs were

used: GFDL-ESM4, IPSL-CM6A-LR, MPI-ESM1–2-HR, MRI-ESM2-0, and UKESM1-0-LL. We refer the reader to Table 3 for a short description of the different scenarios.

Table 3. Table describing expected global warming levels, radiative forcing, and description of SSP-RCP scenarios used in this study.

Scenario	Description
SSP1-RCP2.6	Global warming of 2 ˚C, radiative forcing of 2.6 $W.m^{-3}$ in 2100, presents an optimistic sustainable development with a world where low barriers to mitigation and adaptation are easily overcome and the use of sustainable and green technology is common.
SSP3-RCP7.0	3.6 ˚C global warming, 7.0 $W.m^{-3}$ radiative forcing in 2100, this scenario business as usual world, regional rivalry and low international cooperation with a medium-high emissions pathway and a challenging scenario for mitigation, with significant greenhouse gas emissions and associated climate impacts.
SSP5-RCP8.5	4.4 ˚C global warming, 8.5 $W.m^{-3}$ radiative forcing in 2100, under this pessimistic scenario which represents a world with high economic growth and high dependence on fossil fuels, is characterized by high mitigation challenges due to its dependence on fossil fuels.

Simulations were initiated from the best-fit set of initial conditions. These simulations are further provided with an additional spin-up year to avoid sudden jumps between the initial conditions and simulation start year. All simulations were conducted on Snellius, the Dutch national supercomputer. The MODFLOW6 prototype used in GLOBGM requires substantial preprocessing of the PCR-GLOBWB2 outputs and other relevant inputs into exactly one binary file per unstructured grid. In addition, post-processing is required to convert the binary outputs created during the MODFLOW6 simulation into data formats more commonly used by the community. To streamline the multi-model simulations, the pre-processing, MODFLOW6 simulation, and the post-processing steps were collected into a single snakemake workflow[63] constructed to fit the HPC architecture on Snellius. For GLOBGMv1.0 satisfactory simulation times were achieved when running on 12 compute nodes, and as such each simulation presented here was assigned 12 compute nodes. For the historical reference simulation (1960 - 2019), the total run time was approximately 21 h. Whereas for a single SSP-RCP simulation, with its historical baseline (1960-2014) and three future runs (2015 - 2100), the total simulation time was a single simulation was approximately 106 h.

Data Records

Simulated groundwater heads and water table depths are available on YODA, a research data management service of Utrecht University. For the historical reference simulation (ISIMIP3a) long term averages, annual averages and monthly groundwater head and water table depths are provided. Whereas for the future projections (ISIMIP3b) long-term averages, annual averages are provided per GCM under the three SSP-RCP scenarios. In addition, we provide the ensemble mean for long-term averages, annual averages and monthly estimates of groundwater head and water table depth for the three SSP-RCP scenarios. A data set relating to the quality assurance of the simulated outputs is also available on YODA. Access links are available in Table 4 and instructions and codes for accessing the are available on the following website: https://vanjaarsveldbarry.github.io/globgm_cmip6/.

Table 4. Data Repositories for Water Table Depth and Groundwater Heads Data.

Name	Description	DOI
historical-reference-gswp3-w5e5[64]	Long-term average, annual and monthly water table depth and groundwater heads for the historical reference simulation (ISIMIP 3a).	doi.org/10.24416/UU01-AKSHOX
globgm-cmip6-monthly[65]	Ensemble mean of monthly water table depth and groundwater heads for SSP1-2.6, SSP3-7.0, SSP5-8.5 scenarios over the historical benchmark (1960 - 2014) future periods (2015 - 2100).	doi.org/10.24416/UU01-1BXLPD
globgm-cmip6-annual[66]	Annual water table depth and groundwater heads from individual GCMs and their ensemble mean for the SSP1-2.6, SSP3-7.0, and SSP5-8.5 scenarios, covering the historical (1960–2014) and future (2015–2100) periods	doi.org/10.24416/UU01-V6B9YS
globgm-cmip6-average[66]	Average water table depth and groundwater heads from individual GCMs and their ensemble mean for the SSP1-2.6, SSP3-7.0, and SSP5-8.5 scenarios, covering the historical (1960–2014) and future (2015–2100) periods	doi.org/10.24416/UU01-SLRFI7
globgm-cmip6-quality[67]	Data pertaining to the quality assurance of the simulated outputs	doi.org/10.24416/UU01-16EJ3Y

Data Overview

Mean annual water table depth, from 1960 - 2019, highlights the added detail in representing global groundwater dynamics at the hyper-resolution which better represents spatial variability

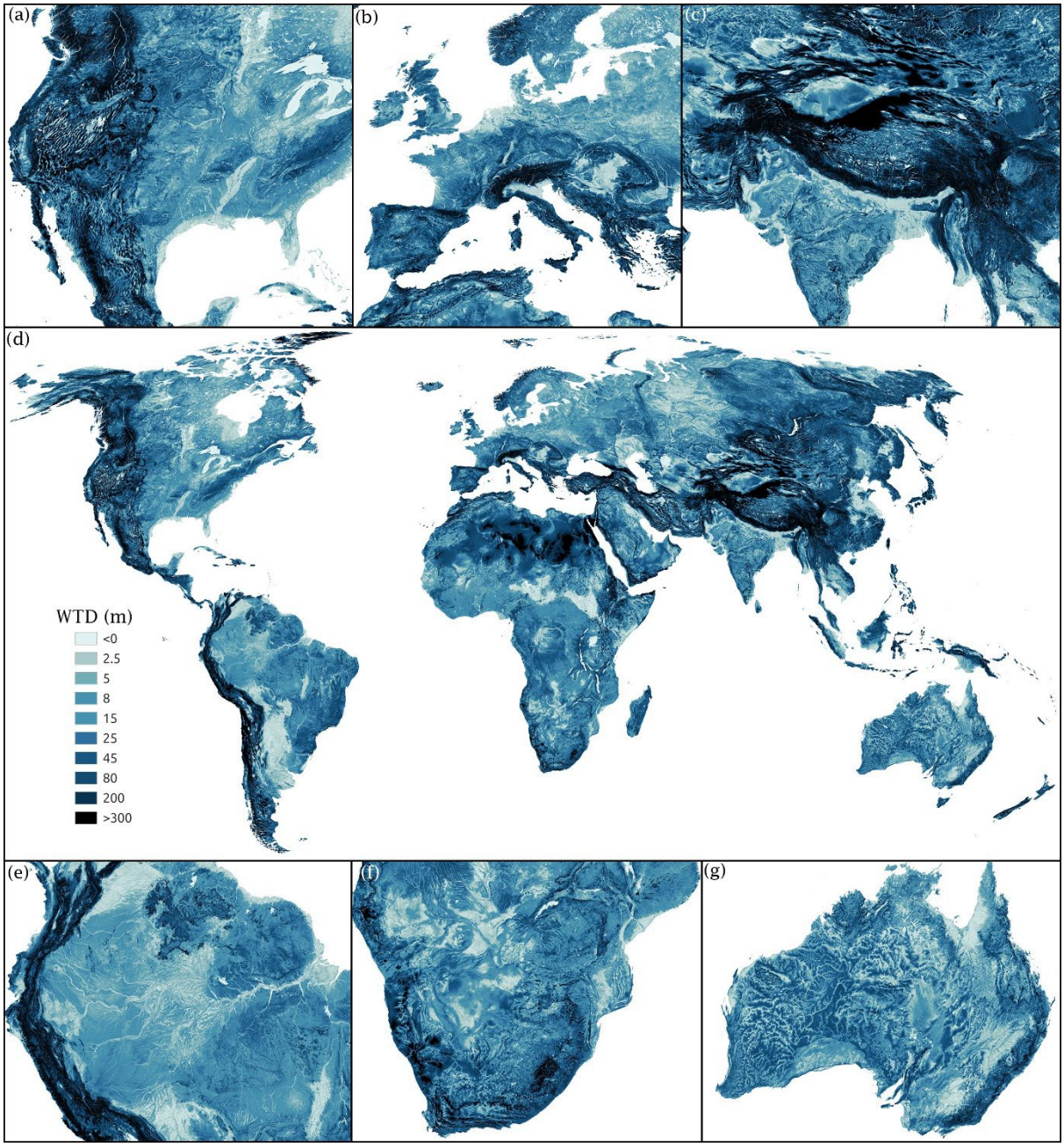

Figure 2. (d) Mean annual water table depth (1960 - 2019) simulated by GLOBGM. With zoomed insets providing more detail over (a) the United States, (b) western Europe, (c) Indo-Gangetic Plain, and (e) the Amazon basin, (f) southern Africa and (g) Australia. In areas where a confining layer is present, only the uppermost model layer is depicted, thus providing a from the ground surface downwards perspective.

(Figure 2a,b,c,d,e,f,g). In addition, finer scale interactions between river systems and groundwater are evident at this hyper-resolution. For instance, the shallow reaches of the Amazon and Mississippi rivers, with their respective deltas, are visible through shallow water tables (Figure 2a,e). Other major deltas such as the Indus and Ganges-Brahmaputra are also well resolved at this resolution (Figure 2c). Average water table depths largely resemble our current broad understanding of groundwater dynamics and reflect the influences of precipitation, topography, and geology on driving the distribution of groundwater reserves.

Water table depths are seen to be deeper in the arid regions and shallower in humid areas; reflecting the difference in groundwater recharge rates which is driven by large scale precipitation patterns[68]. In addition, more mountainous regions exhibit deeper water table depths which is expected given the relatively lower infiltration rates, through lower permeability, of these regions and tendency for water to move down slope towards lower lying ground under the influence of gravity[69]. Additionally, there are shallower depths of the water table along the coast line on comparison to more interior regions.

Technical Validation

Calibration

GLOBGM showed sensitivity to different factor adjustments for parameters that were subject to calibration; namely, hydraulic conductivity, anisotropy, and entrance resistance (Figure 3 & Table 5). Given that global groundwater models are more accurate in predicting groundwater reserves that are shallower compared to reserves that are deeper and that shallower groundwater (< 60 m) is arguably more important to maintain ecosystem integrity through groundwater discharge into streams and groundwater dependent wetlands, and people through abstractions[32,40,68,70]. Furthermore, the disagreement of the model ensembles correlates with the depth of groundwater, and the predecessor to GLOBGM was shown to have a lower accuracy in predicting deeper depths compared to shallower water table depths[21,32,35,40], presumably due to uncertainties in geological parametrisation of the deeper sub-surface[71]. Therefore, we selected the best set of calibration settings 405 according to depth class so that accuracy of shallower water table depths is prioritised.

Water table depth biases were calculated for each depth class, and the average of these classes was used to obtain an overall bias for each calibration permutation. Calibration permutations were ordered as a function of average depth weighted bias, and the top ten were selected to choose a subset of permutations that resulted in the best overall performance. From these top ten, the prefactor combination that displayed the best accuracy for the 0-5m depth category is also the combination that displays the best accuracy overall and for the 10-20m depth category, while still displaying the second best accuracy for the 5-10m depth category (Table 5). As such, a prefactor of 0.1 for all parameters was chosen as the best set. The fact that the selected prefactors correspond to the minimum values tested suggests that smaller prefactors may have provided better performance. However, the range of tested prefactors was limited to within two

orders of magnitude to avoid significant deviations from the original model parametrisation and over-fitting and reductions in the model's ability to generalize beyond the calibration data.

Table 5. Table showing the top 3 calibration candidates (when ordered by mean depth weighted bias) and their associated parameter settings and mean bias per depth class. For reference, the final row contains the bias score calculated from GLOBGMv1.0. FCU: Fine + Coarse unconsolidated, FCC: Fine + Coarse consolidated, Carb: Carbonate.

Variable					Bias (m)						
Ks			Anisotropy	Entrance Resistance	<0	0-5	5-10	10-20	20-60	>60	mean
FCU	FCC	Carb									
0.1	0.1	0.1	0.1	0.1	37.3	9.6	12.0	15.6	27.2	93.3	32.5
0.1	0.1	0.1	1.0	0.1	37.7	9.7	11.9	15.4	27.0	93.1	32.5
0.1	1.0	0.1	0.1	0.1	37.6	9.8	12.3	15.9	27.2	92.7	32.6
GLOBGMv1.0					41.3	13.6	17.1	20.4	27.3	85.6	34.2

Comparing the cumulative distribution of bias across observation wells shows that there is greater variance amongst permutations for locations where the simulated depth of the water table is deeper than observed - suggesting that calibration had a relatively greater influence on estimations of simulated water tables depths that were too deep in comparison to estimations that simulated water tables depths that were too shallow (Figure 3e). Additionally, varying calibration prefactors tended to shift the entire distribution to either more positive or negative bias and did not solely correct the outliers at either end of the distribution simultaneously (Figure 3e). When inspecting the cumulative distribution of bias for the chosen best set of prefactors, it's clear that these set of prefactors result in a more accurate estimation of water table depths that tend to be simulated too deep (Figure 3e) which as a result meant that water table depths that tend to be simulated as too shallow were penalized (Figure 3e). However, it is important to note that this set of prefactors also resulted in the best overall bias (Table 5), where it is clear from Figure 5e that the gains at the negative end of the distribution are offset by penalties at the positive end of the distribution. In comparison to the previous uncalibrated version of GLOBGM[38], we see that the chosen set of calibration setting display marked reductions in overall depth-weighted bias. This is especially prevalent for shallower water table depths (<0 - 20 m; Table 5). For deeper water table depths, calibration had little impact for wells between 20 and 60 m and was less accurate for wells deeper than 60 m. The mean bias compared to the previous GLOBGM version shifts from a tendency to overestimate water table depths (-4.8 m) to an underestimation when calibrated (3.6 m) considering all 430 observation wells (Figure 3e,f). However, bias in the calibrated model is closer to the ideal number of zero

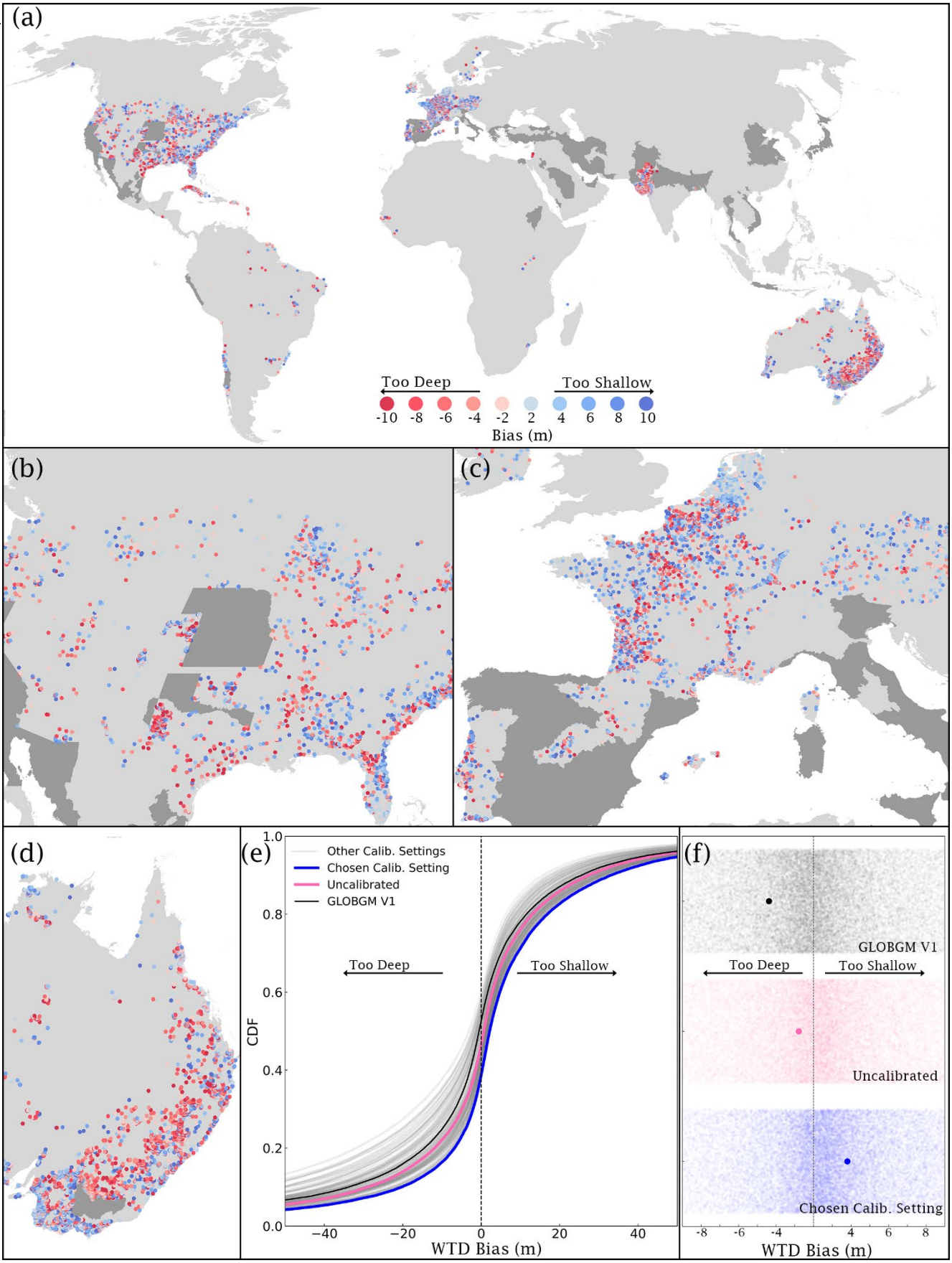

Figure 3. (a) Geographical variation of water table depth bias from 34,800 observation used for calibration. Grey polygons indicate excluded regions of known anthropogenic influence. Zoomed insets of the (b) United States, (c) western Europe, (d) Australia. (e) Cumulative distribution function of the water table depth bias of the 163 permutations. (f) A mean points plot showing the mean water table depths for the uncalibrated, chosen permutation and GLOBGMv1.0. Points are distributed along the y axis to better visualise the spread of data, therefore the y axis is not quantitative.

by approximately 1 metre (Figure 3e,f). This analysis also allows for inference on how the addition of the saturated area fraction correction and groundwater recharge affects the models predictive ability. The un-calibrated predictions where closer (-1.6 m) to the ideal bias score of zero when compared to the previous version of GLOBGM (-4.8 m), again centred around improvements in the wells that were deeper than observed, indicating that these additions improved the models accuracy (Figure 3e,f).

Initial conditions estimation

The spin up procedure followed here has significant effects on the initial heads estimates for the simulation start year. Groundwater heads were the highest after the steady state simulation step and progressively decreased during the two transient simulation steps, the first without pumping followed by the inclusion of pumping (Figure 4). During the three spin up steps, the overall change in average heads was comparable, when averaged across sub-models, for the upper and lower layer - 4.9 m and 5.5 m, respectively(Figure 4). However, differences between the sub-models were evident. For the upper model layer, the change in heads was comparable

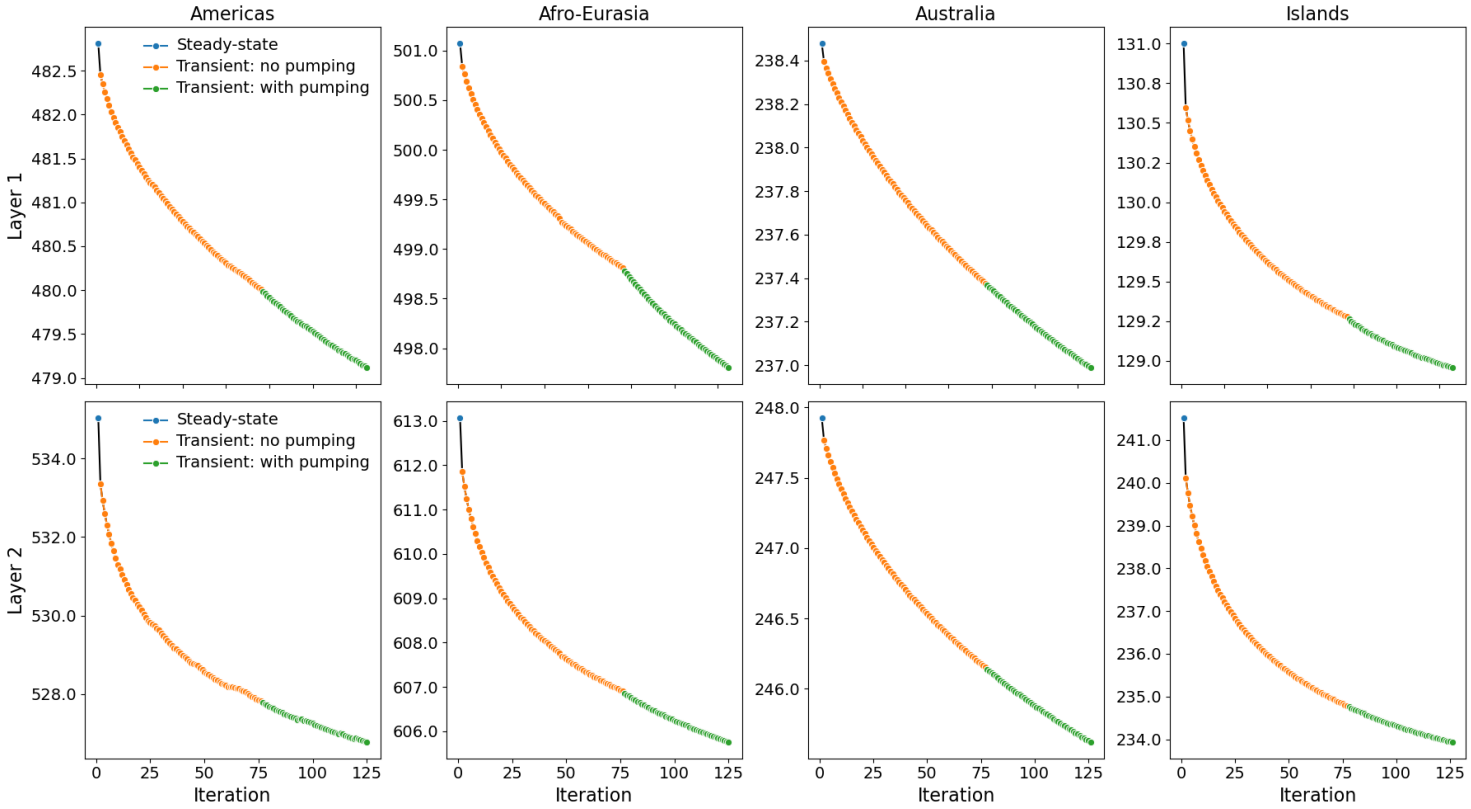

Figure 4. Change in average groundwater head during initial conditions estimation over the four independent sub-models, starting from the steady state estimates, followed by a transient simulation for 1960 with no pumping, and concluded by a transient simulation for 1960 with pumping.

for the Americas (3.3 m) and Afro-Eurasia sub-model (3 m). Whilst, Australia (1.4 m) and the Islands (2 m) sub-models displayed a smaller degree of change in average groundwater heads (Figure 4). The Americas (6 m), Afro-Eurasia (7 m), and Islands (7 m) sub-models were comparable for the lower layer, with Australia (2 m) displaying a significantly smaller change in average groundwater heads (Figure 4).

The objective of the first transient spin up step was to achieve dynamic equilibrium for the year 1960. Whereas, the objective of the second transient spin up step was to reproduce the expected groundwater heads for 1960 by activating abstraction. The key assumption here is that groundwater heads calculated from steady state solution and simulating 1960 iteratively, without abstraction, would yield groundwater heads that were greater than observed and as such by activating abstraction groundwater heads in the second spin up step would allow for the groundwater heads to approach observed values. During the first spin up step without abstraction, the change in average groundwater heads between successive iterations decreased as the number of iterations increased (Figure 4) - suggesting that the model approached a dynamic equilibrium. One reason the average groundwater heads at the continual scale did not display strict states of dynamic equilibrium may be that a relatively small number of grid cells were not in equilibrium. This notion is challenging to prove at the global-scale given the small number and highly clustered distribution of observation stations present for 1960 (Figure 5a). However, when evaluating the first spin up step for where observations were present, there is evidence that states of dynamic equilibrium were achieved (Figure 5b). For the second transient spin up step, average bias and average relative bias decreased in both model layer for the Afro-Eurasia and Islands sub-models and approached observed water table depths (Figure 5b). However, for the Americas sub-model average bias values improved as iterations increased whilst average relative bias deteriorated as iterations increased (Figure 5a), a result explainable by the disproportionate influence of a limited number of outliers. The changes in groundwater head with respect to observation wells that were present in 1960 reveal that the spin-up without abstraction did indeed reach states of dynamic equilibrium and that during the second transient spin up step, bias approached zero (Figure 5b), suggesting that the model approached more accurate initial estimates for groundwater heads. Interestingly, there is a clear difference when it comes to model layer and tendencies towards points of diminishing returns during the first transient spin up step: the lower model layer displayed a more muted change in average groundwater head in comparison to the upper model layer (Figure 4). Similarly, the transient simulation with pumping also showed decreases in change between iterations as the number of

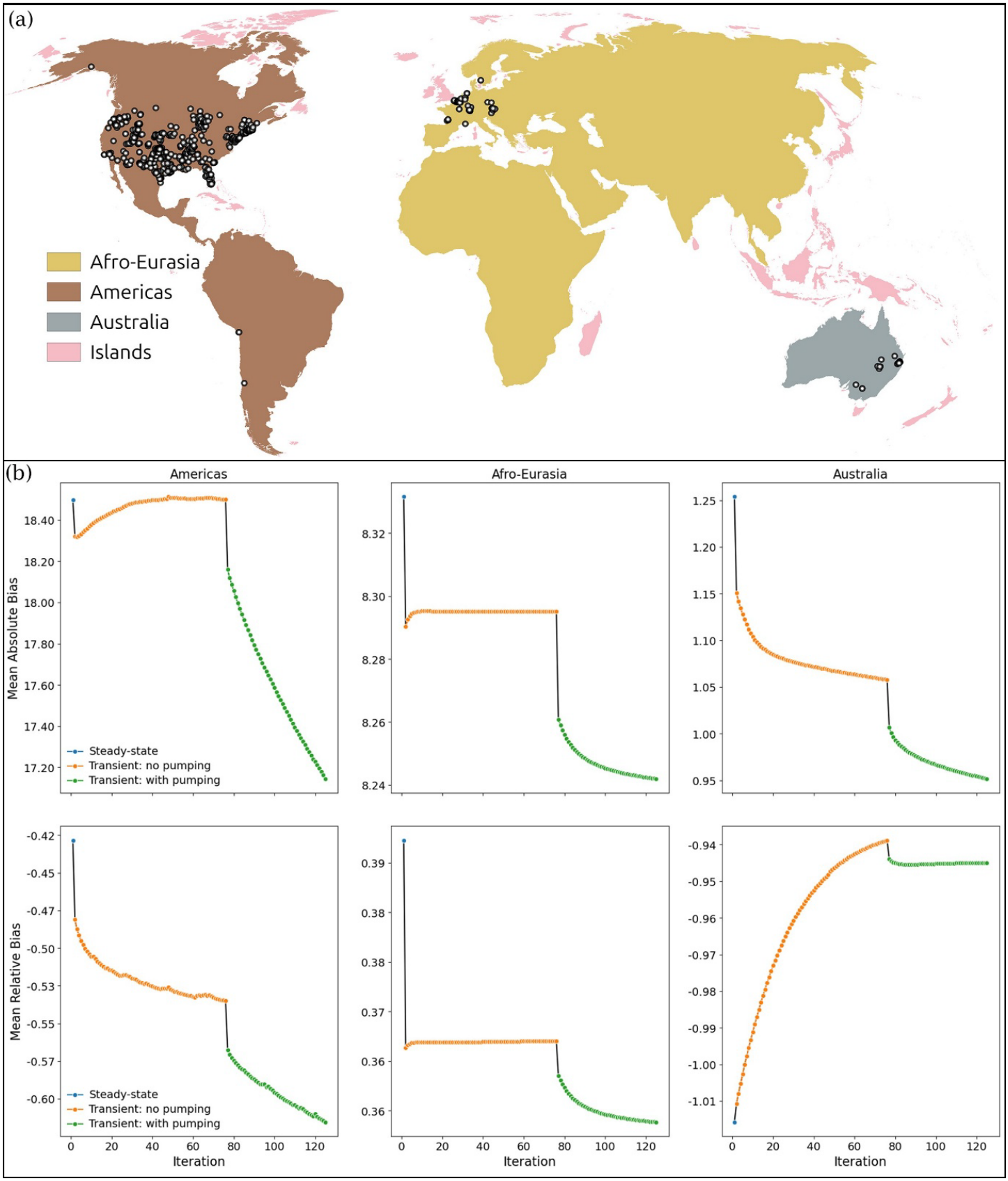

Figure 5. (a) Locality of 2.175 stations for 1960 used during the initial conditions simulations. The evolution of the (b) mean absolute and mean relative bias calculated from the simulated water table depth and observed water table depths of a set number of iterations. Note that the islands model did not have enough data for this step.

iterations increased and again the lower layer displayed less change between iterations as the number of iterations increased (Figure 4). This difference between the upper and lower model layers may be related to the fact that lower hydraulic conductivities and transmissivity of deeper aquifers, meaning that changes on the land cover related to groundwater recharge and anthropogenic abstractions have a slower response time for these deeper regions. In addition, the effect of a confining layer will further delay the response and isolate the confined layer from direct land surface dynamics and only changes through vertical flows which are relatively small.

Historical Validation:

The simulated monthly water table depths were evaluated against observed water table depths obtained from IGRAC's Global Groundwater Monitoring Network. Data were filtered so that all observations contain a minimum of 60 months of groundwater observations, which results in a total of 40.846 observation wells. The Kling-Gupta Efficiency (Equation 8) was used to assess the accuracy of the simulated values against the observed data. KGE values range from -∞ to 1.0, with values greater than -0.41 implying that the model is a better predictor than the mean of the data[72]. To match the observed data to the correct model layer, the same procedure relying on correlations between soil moisture and simulated water table depths was used for calibration and initial condition estimation.

$$KGE = 1 - \sqrt{(\rho - 1)^2 + (\alpha - 1)^2 + (\beta - 1)^2} \quad (8)$$

Where ρ is the Pearson's correlation coefficient between the simulated and observed time series, α is the variability ratio, defined as the ratio of the standard deviation of the simulations to that of the observations, and β the bias ratio, defined as the ratio of the mean of the simulations to the mean of the observations.

Evaluating transient monthly predictions of groundwater table depth against observation wells reveals that approximately 45% of the simulated water table depths for which there are observed data are skilful, when using a KGE threshold of -0.41 (Figure 6a). When considering the different constituents of the KGE score, 85 % of the evaluated points display a correlation greater than 0.0 (Figure 6b), almost all points display a variability in monthly water table depth that is lower than observed time series (Figure 6c). Whereas, the ability of the model tends to predict long-term monthly mean water table depths which are shallower than observed (Figure 6d).

The ability of GLOBGM to simulate water table depths varies considerably with the depth. KGE scores grouped according to the depth categories reveal that the worst performing category is water table depths that are 0-5 m and deeper than 60 m, with approximately 55 % of locations that display a KGE greater than -0.41, which is indicative skilful predictions that improve upon the mean flow benchmark (Figure 6e). The depths between 5 and 60 m are simulated with the highest accuracy where between 55 and 65 % of observations display skilful results (Figure 6e). The ability of reproduce correlations shows a clear pattern with depth, where shallower values are more accurately predicted than deep and above ground water table depths (Figure 6f). Whereas, the ability to reproduce variability in water table depth shows no clear correlation with depth of observed groundwater in terms of average variance ratio or the bias of the variance ratio (Figure 6g). Water table depths tends to be underestimated where observations are between 0 - 5 m (Figure 6h). The bias is closest to 0 for the 5 - 10 m class and tends to be overestimated for deeper wells and underestimated for wells deeper than 10 m (Figure 6h).

The spatial variation in KGE score corroborates some of the conclusions derived from the cumulative distribution functions in Figure 7, for example, higher KGE values are evident along the coast where water table depths are shallower (Figure 7a). Furthermore, the effect of depth becomes evident when comparing relatively lower KGE scores in the higher elevations of the Appalachian, Pyrenees and Great Divide mountains to higher scores in the adjunct low lying regions (Figure 7b). Similarly, the higher regions of the Indo-Gangetic plain display lower KGE values compared to more coastal points (Figure 7b,c,d).

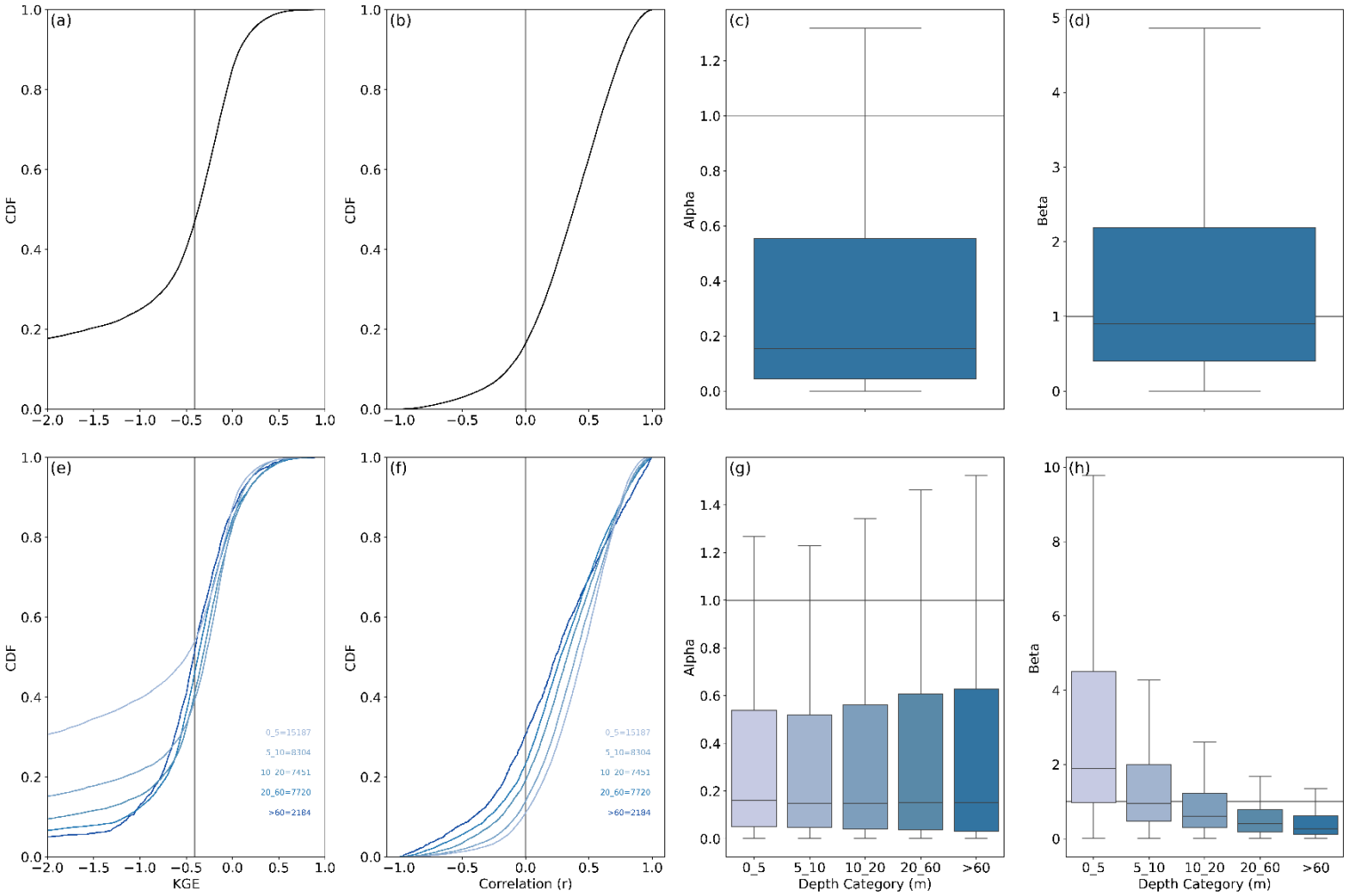

Figure 6. Panels a-d represent the values of all the observation points whilst panels e-g represent the same set of observation points but separated according to depth class. (a, e) KGE and its constituent components (b, f) correlation, (c, g) beta, and (d, e) alpha calculated for monthly water table depth simulated by GLOBGM from 1960–2019. Gray lines in (a, e) symbolises a KGE of -0.41 which is indicative of predictions that improve upon the mean flow benchmark. Gray lines in (b, f) indicate the point at which correlations to the right are positive and to the left are negative, in (c, g) the point at which alpha represents overestimation upwards and underestimations downwards, and (d, h) the point at which beta represents overestimation upwards and underestimations downwards.

521

522

523

524

525

526

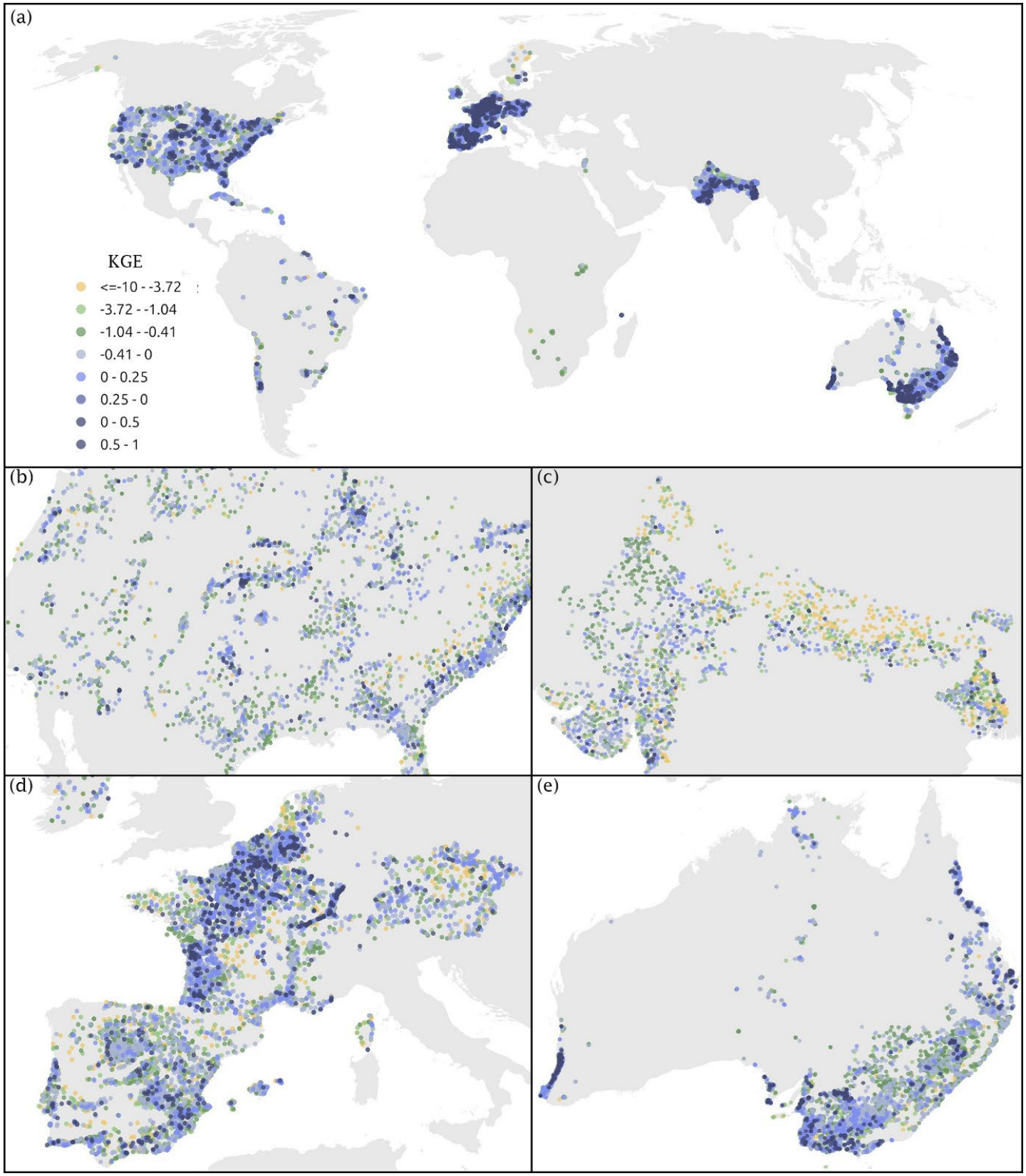

Figure 7. (a) Spatial distribution of KGE scores calculated from monthly water table depth simulated by GLOBGM from 1960–2019. With zoomed insets providing more detail for the (b) United States, (c) western Europe, (d) Indo-Gangetic Plain and (e) Australia. KGE values greater that -0.41 are indicative of predictions that improve upon the mean flow.

Usage Notes

In addition to the evaluation based on water table depth observations, we provide a map of regions where predictions are likely less accurate or likely to fall outside the range of applicability of a GLOBGMv1.1 (Figure 9). In summary, GLOBGM and its predecessor have been shown to yield less accurate results in regions dominated by mountainous terrain, permafrost, and karst aquifers[35,38,73]. To facilitate inquiries using the groundwater data presented here that considers their known uncertainties, we provide a quality assurance dataset containing gridded information on potential sources of uncertainty. Regions dominated by karst aquifer systems were obtained from the World Karst Aquifer Map (WHYMAP WOKAM)[74] and rasterised to match the grid resolution used in GLOBGM. The Global Permafrost Zonation Index Map was used to identify regions that are dominated by permafrost in almost all conditions using a threshold value of 0.9; which corresponds to regions where there is permanent and continuous permafrost[75,76]. For the identification of mountainous regions, we used the standard deviation of slope within each grid cell of the GLOBGM dataset. A threshold value of 77 was established to delineate mountainous terrain. This threshold corresponds to the 99th percentile, indicating that grid cells with slope standard deviation values exceeding 77 belong to the top 1% in terms of topographical heterogeneity.

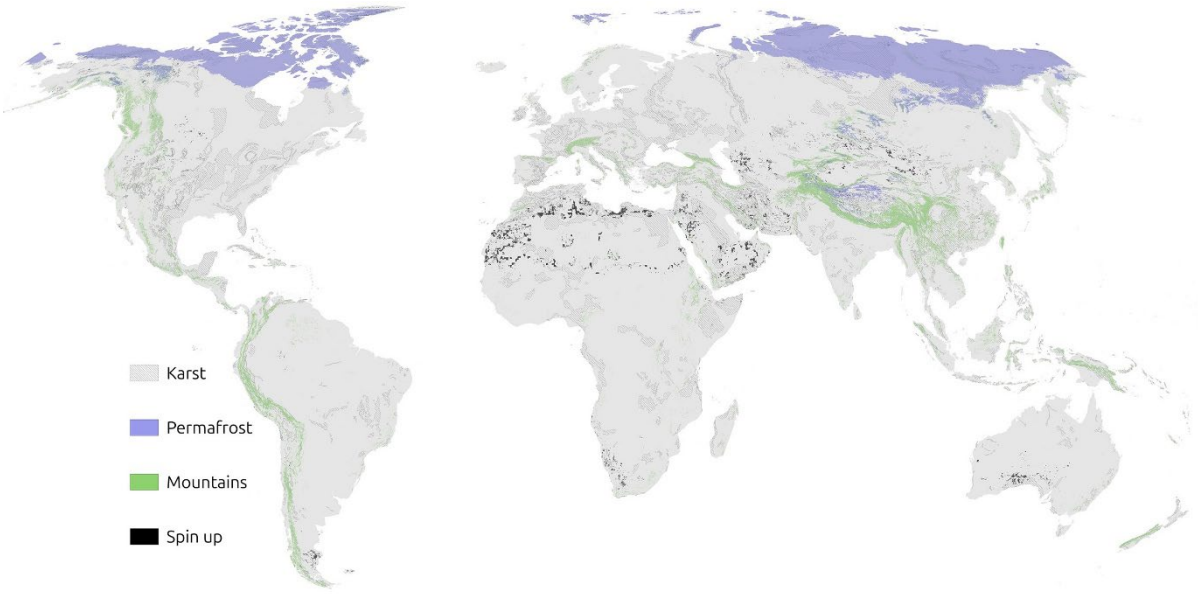

Figure 9. Regions where GLOBGM has been shown to provide less accurate results due to practical and theoretical limitations; namely, karst aquifers, permafrost and mountainous regions. In addition, regions where spin up issues are prevalent are also indicated.

In addition, we evaluate the prevalence of grid cells that did not undergo proper initialisation of starting heads through the initial condition estimation procedure. If the initial heads estimates used as starting points for the simulations were not at dynamic equilibrium, spurious trends in groundwater heads or water table depths will be evident. To identify whether trends were a result of insufficient spin up when deriving initial states, we evaluated the trends in groundwater in relation to trends in groundwater recharge and whether or not abstraction is present in that cell, for a single GCM (IPSL-CM6A-LR), which is intermediate among the 5 models in terms of global temperature and precipitation change, over the entire simulation period (1960 - 2100) for the business as usual scenario. Based on a first principles understanding of groundwater dynamics we identified two combinations which are improbable and suggest that trends in groundwater heads are due to insufficient spin up (Figure 10). However, this would not provide information on when in the time series potential spin up issues would end, and as such we repeated this analysis for different time periods (1990 - 2100, 2020 - 2100; 2070 - 2100) in order to provide users with information on when and where spin up issues are resolved. Regarding the accuracy of predictions in mountainous regions, GLOBGM models groundwater heads within the mountain blocks but does not parametrize for water bodies in hill slopes and smaller alluvial mountain valleys, since the hydrogeological schematization is too coarse in these regions. Moreover, it is assumed that the secondary permeability of fractured hard rock in mountainous regions can also be represented by the principles of Darcian groundwater flow[38]. Research on the applicability of PCR-GLOBWB2 to simulate the hydrology of permafrost regions shows that it does not capture the dynamics of permafrost with high fidelity due to its simplistic representation of ice melt (i.e., degree-day factor) and lack of dynamic permafrost schemes leads to underestimated discharge and by proxy groundwater recharge[73]. Moreover, it is challenging to define groundwater resources in areas where soil is frozen up to many tenths of meters deep[77,78]. To facilitate uncertainty-informed use of the groundwater data provided here, we provide users with a quality assurance raster pertaining to regions with karst, permafrost, or that are mountainous

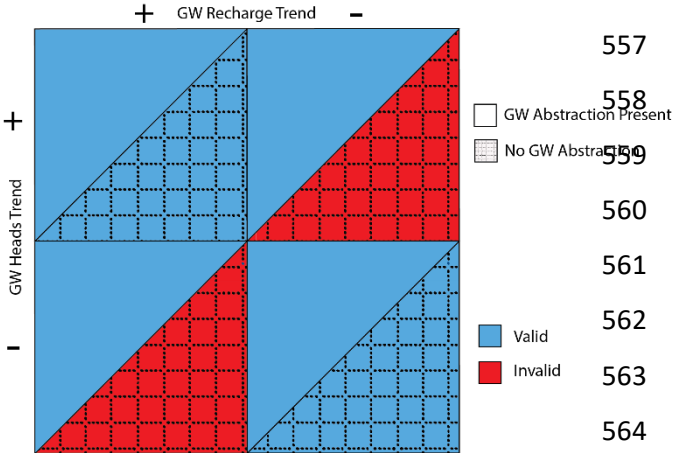

Figure 10. Matrix diagram showing combinations of trends in groundwater (GW) heads, recharge and the presence of abstraction and classification combinations according validity.

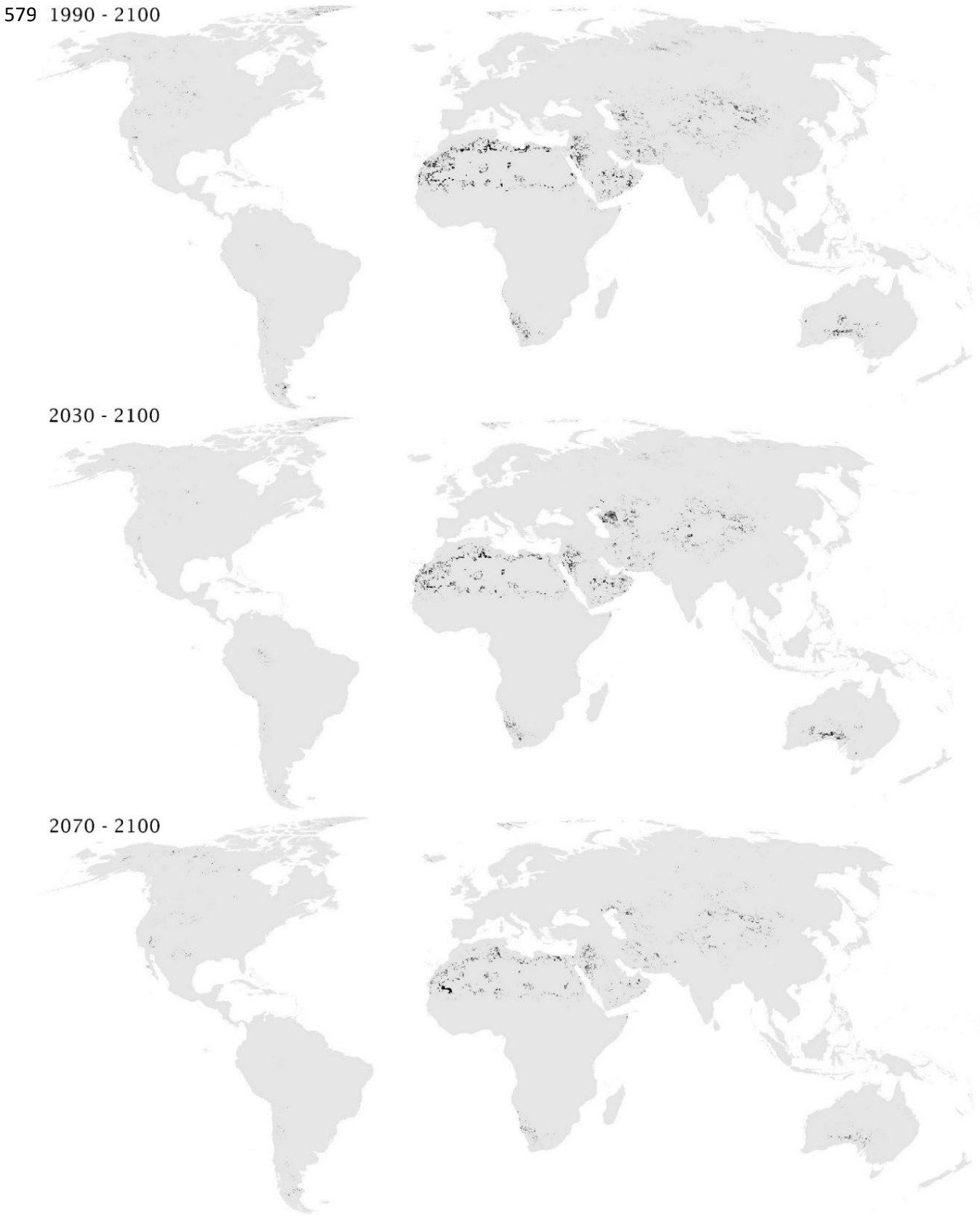

Figure 11. Regions where the model estimates are known to be affected by spin up issues for the entire simulation period (1960–2100) and isolates effects persisting into the last 60 years (2030–2100) and last 30 years (2070–2100) of the projection.

regions (Figure 9). In addition to this static quality assurance, we provide users with the regions for which spin up issues were detected over the entire simulation period (1960 - 2100, Figure 9) and different subsets to provide users with information on when and where spin up issues are resolved (1990 - 2100, 2020 - 2100; 2070 - 2100; Figure 11).

Data Availability

Simulated groundwater heads and water table depths are available on YODA, a research data management service of Utrecht University. For the historical reference simulation (ISIMIP3a) long term averages, annual averages and monthly groundwater head and water table depths are provided. Whereas for the future projections (ISIMIP3b) long term averages, annual averages are provided per GCM under the three SSP-RCP scenarios. In addition, we provide ensemble long term averages, annual averages and monthly estimates of groundwater head and water table depth for the three SSP-RCP scenarios. A data set relating to the quality assurance of the simulated outputs is also available on YODA. historical-reference-gswp3-w5e5: https://doi.org/10.24416/UU01-AKSHOX, globgm-cmip6-monthly: https://doi.org/10.24416/UU01-1BXLPD, globgm-cmip6-annual: https://doi.org/10.24416/UU01-V6B9YS, globgm-cmip6-average: https://doi.org/10.24416/UU01-SLRFI7, globgm-cmip6-quality: https://doi.org/10.24416/UU01-16EJ3Y.

Code Availability

Model code used to run simulations has been archived on Zenodo and can be accessed here at the following link: https://doi.org/10.5281/zenodo.17065147.

Acknowledgements

This work made use of the Dutch national e-infrastructure with the support of the SURF Cooperative (using grant no. EINF-11758 , EINF-9757 & NWO-2024.031). MB acknowledges support from the ERC Advanced Grant scheme (Grant no. 101019185 – GEOWAT). Myrthe Leijnse is thanked for guidance in accessing and using the hotspot polygons. Maisam Mohammadi Dadkan and Vincent Brunst are thanked for their guidance and assistance with hosting the data on YODA.

Authors Contributions

BvJ: Data curation, Formal analysis, Software, Validation, Visualization, Writing – original draft preparation. **NW:** Conceptualization, Project administration, Supervision, Writing – review & editing. **NGO:** Conceptualization, Data curation, Software, Writing – review & editing. **JV:** Data curation, Software, Writing – review & editing. ES: Conceptualization, Data curation, Software, Writing – review & editing. **DZ:** Conceptualization, Data curation, Writing – review & editing. **MB:** Conceptualization, Funding acquisition, Project administration, Resources, Supervision, Writing – review & editing.

Competing Interests

The authors have no other competing interests to declare.

References

1. Döll, P. *et al.* Impact of water withdrawals from groundwater and surface water on continental water storage variations. *Journal of Geodynamics* **59–60**, 143–156 (2012).
2. Gleeson, T., Cuthbert, M., Ferguson, G. & Perrone, D. Global Groundwater Sustainability, Resources, and Systems in the Anthropocene. *Annual Review of Earth and Planetary Sciences* **48**, 431–463 (2020).
3. Custodio, E. Intensive groundwater development: A water cycle transformation, a social revolution, a management challenge. in *Re-thinking Water and Food Security* (CRC Press, 2010).
4. Bierkens, M. F. P. & Wada, Y. Non-renewable groundwater use and groundwater depletion: a review. *Environmental Research Letters* **14**, 063002 (2019).
5. Niazi, H. *et al.* Global peak water limit of future groundwater withdrawals. *Nature Sustainability* **7**, 413–422 (2024).
6. Wada, Y. & Bierkens, M. F. P. Sustainability of global water use: past reconstruction and future projections. *Environmental Research Letters* **9**, 104003 (2014).
7. Kuang, X. *et al.* The changing nature of groundwater in the global water cycle. *Science* **383**, eadf0630 (2024).
8. Rodell, M. *et al.* Emerging trends in global freshwater availability. *Nature* **557**, 651–659 (2018).

9. Leijnse, M. *et al.* Key drivers and pressures of global water scarcity hotspots. *Environmental Research Letters* **19**, 054035 (2024).
10. Wada, Y. *et al.* Global depletion of groundwater resources. *Geophysical Research Letters* **37**, 2010GL044571 (2010).
11. Taylor, R. G. *et al.* Ground water and climate change. *Nature Climate Change* **3**, 322–329 (2013).
12. Moeck, C. *et al.* A global-scale dataset of direct natural groundwater recharge rates: A review of variables, processes and relationships. *Science of The Total Environment* **717**, 137042 (2020).
13. Maples, S. R., Fogg, G. E. & Maxwell, R. M. Modeling managed aquifer recharge processes in a highly heterogeneous, semi-confined aquifer system. *Hydrogeology Journal* **27**, 2869–2888 (2019).
14. Ilstedt, U. *et al.* Intermediate tree cover can maximize groundwater recharge in the seasonally dry tropics. *Scientific Reports* **6**, 21930 (2016).
15. West, C., Rosolem, R., MacDonald, A. M., Cuthbert, M. O. & Wagener, T. Understanding process controls on groundwater recharge variability across Africa through recharge landscapes. *Journal of Hydrology* **612**, 127967 (2022).
16. Vörösmarty, C. J., Green, P., Salisbury, J. & Lammers, R. B. Global Water Resources: Vulnerability from Climate Change and Population Growth. *Science* **289**, 284–288 (2000).
17. Jasechko, S. *et al.* Rapid groundwater decline and some cases of recovery in aquifers globally. *Nature* **625**, 715–721 (2024).
18. Jasechko, S. & Perrone, D. Global groundwater wells at risk of running dry. *Science* **372**, 418–421 (2021).
19. Perrone, D. & Jasechko, S. Deeper well drilling an unsustainable stopgap to groundwater depletion. *Nature Sustainability* **2**, 773–782 (2019).
20. De Graaf, I. E. M., Marinelli, B. & Liu, S. Global analysis of groundwater pumping from increased river capture. *Environmental Research Letters* **19**, 044064 (2024).

21. Xie, J. *et al.* Majority of global river flow sustained by groundwater. *Nat. Geosci.* **17**, 770–777 (2024).
22. Bierkens, M. F. P., Sutanudjaja, E. H. & Wanders, N. Large-scale sensitivities of groundwater and surface water to groundwater withdrawal. *Hydrology and Earth System Sciences* **25**, 5859–5878 (2021).
23. Saccò, M. *et al.* Groundwater is a hidden global keystone ecosystem. *Global Change Biology* **30**, e17066 (2024).
24. Fan, Y., Miguez-Macho, G., Jobbágy, E. G., Jackson, R. B. & Otero-Casal, C. Hydrologic regulation of plant rooting depth. *Proceedings of the National Academy of Sciences* **114**, 10572–10577 (2017).
25. Otoo, N. G., Sutanudjaja, E. H., Van Vliet, M. T. H., Schipper, A. M. & Bierkens, M. F. P. Mapping groundwater-dependent ecosystems using a high-resolution global groundwater model. *Hydrol. Earth Syst. Sci.* **29**, 2153–2165 (2025).
26. Huggins, X. *et al.* Groundwater Connections and Sustainability in Social-Ecological Systems. *Groundwater* **61**, 463–478 (2023).
27. Garrick, D. E. *et al.* Valuing water for sustainable development. *Science* **358**, 1003–1005 (2017).
28. *Groundwater Making the Invisible Visible*. (UNESCO, Paris, 2022).
29. Condon, L. E. *et al.* Global Groundwater Modeling and Monitoring: Opportunities and Challenges. *Water Resources Research* **57**, e2020WR029500 (2021).
30. Bäthge, A. *et al. GROW: A Global Time Series Dataset for Large-Sample Groundwater Studies*. https://meetingorganizer.copernicus.org/EGU25/EGU25-17713.html (2025) doi:10.5194/egusphere-egu25-17713.
31. Zamrsky, D. *et al.* Current trends and biases in groundwater modelling using the community-driven groundwater model portal (GroMoPo). *Hydrogeology Journal* **33**, 355–366 (2025).
32. Fan, Y., Li, H. & Miguez-Macho, G. Global Patterns of Groundwater Table Depth. *Science* **339**, 940–943 (2013).

33. Reinecke, R. *et al.* Challenges in developing a global gradient-based groundwater model (G^3M v1.0) for the integration into a global hydrological model. *Geoscientific Model Development* **12**, 2401–2418 (2019).
34. Costantini, M., Colin, J. & Decharme, B. Projected Climate-Driven Changes of Water Table Depth in the World's Major Groundwater Basins. *Earth's Future* **11**, e2022EF003068 (2023).
35. de Graaf, I. E. M. *et al.* A global-scale two-layer transient groundwater model: Development and application to groundwater depletion. *Advances in Water Resources* **102**, 53–67 (2017).
36. Bierkens, M. F. P. Global hydrology 2015: State, trends, and directions. *Water Resources Research* **51**, 4923–4947 (2015).
37. Wood, E. F. *et al.* Hyperresolution global land surface modeling: Meeting a grand challenge for monitoring Earth's terrestrial water. *Water Resources Research* **47**, 2010WR010090 (2011).
38. Verkaik, J., Sutanudjaja, E. H., Oude Essink, G. H. P., Lin, H. X. & Bierkens, M. F. P. GLOBGM v1.0: a parallel implementation of a 30 arcsec PCR-GLOBWB-MODFLOW global-scale groundwater model. *Geosci. Model Dev.* **17**, 275–300 (2024).
39. Rosenzweig, C. *et al.* Assessing inter-sectoral climate change risks: the role of ISIMIP. *Environmental Research Letters* **12**, 010301 (2017).
40. Reinecke, R. *et al.* Uncertainty in model estimates of global groundwater depth. *Environmental Research Letters* **19**, 114066 (2024).
41. Reinecke, R. *et al.* The ISIMIP Groundwater Sector: A Framework for Ensemble Modeling of Global Change Impacts on Groundwater. *EGUsphere* 1–30 (2025) doi:10.5194/egusphere-2025-1181.
42. Huggins, X. *et al.* A review of open data for studying global groundwater in social-ecological systems. (2025).
43. Sutanudjaja, E. H. *et al.* PCR-GLOBWB 2: a 5 arcmin global hydrological and water resources model. *Geoscientific Model Development* **11**, 2429–2453 (2018).

44. Lehner, B., Verdin, K. & Jarvis, A. New Global Hydrography Derived From Spaceborne Elevation Data. *Eos, Transactions American Geophysical Union* **89**, 93–94 (2008).
45. Gnann, S. *et al.* Functional relationships reveal differences in the water cycle representation of global water models. *Nature Water* **1**, 1079–1090 (2023).
46. Berghuijs, W. R. *et al.* Groundwater recharge is sensitive to changing long-term aridity. *Nature Climate Change* **14**, 357–363 (2024).
47. Servén, D., Brummitt, C., Abedi, H., & hlink. dswah/pyGAM: v0.8.0. (2018) doi:10.5281/zenodo.1476122.
48. Mohan, C., Western, A. W., Wei, Y. & Saft, M. Predicting groundwater recharge for varying land cover and climate conditions – a global meta-study. *Hydrology and Earth System Sciences* **22**, 2689–2703 (2018).
49. Brun, P., Zimmermann, N. E., Hari, C., Pellissier, L. & Karger, D. N. Global climate-related predictors at kilometer resolution for the past and future. *Earth System Science Data* **14**, 5573–5603 (2022).
50. Brun, P., Zimmermann, N. E., Hari, C., Pellissier, L. & Karger, D. N. CHELSA-BIOCLIM+ A novel set of global climate-related predictors at kilometre-resolution. (2022) doi:10.16904/ENVIDAT.332.
51. Moeck, C. *et al.* Data for: A global-scale dataset of direct natural groundwater recharge rates: A review of variables, processes and relationships. (2020) doi:10.25678/0001NG.
52. Zomer, R. J., Xu, J. & Trabucco, A. Version 3 of the Global Aridity Index and Potential Evapotranspiration Database. *Scientific Data* **9**, 409 (2022).
53. Poggio, L. *et al.* SoilGrids 2.0: producing soil information for the globe with quantified spatial uncertainty. *SOIL* **7**, 217–240 (2021).
54. Sutanudjaja, E. H. HYPFLOWSCI6: HYdrological Projection of Future gLObal Water States with CMIP6. (2024) doi:10.24416/UU01-YM7A5H.

55. Hagemann, S. & Gates, L. D. Improving a subgrid runoff parameterization scheme for climate models by the use of high resolution data derived from satellite observations. *Climate Dynamics* **21**, 349–359 (2003).
56. Todini, E. The ARNO rainfall—runoff model. *Journal of Hydrology* **175**, 339–382 (1996).
57. Zell, W. O. & Sanford, W. E. Calibrated Simulation of the Long-Term Average Surficial Groundwater System and Derived Spatial Distributions of its Characteristics for the Contiguous United States. *Water Resources Research* **56**, e2019WR026724 (2020).
58. Hartmann, J. & Moosdorf, N. The new global lithological map database GLiM: A representation of rock properties at the Earth surface. *Geochem Geophys Geosyst* **13**, 2012GC004370 (2012).
59. IGRAC. The Global Groundwater Monitoring Network (GGMN). (2024) doi:10.58154/6Z0Y-DA34.
60. Lange, S. & Büchner, M. ISIMIP3b bias-adjusted atmospheric climate input data. (2021) doi:10.48364/ISIMIP.842396.1.
61. Kuzma, S. *et al. Aqueduct 4.0: Updated Decision-Relevant Global Water Risk Indicators*. https://www.wri.org/research/aqueduct-40-updated-decision-relevant-global-water-risk-indicators (2023).
62. Lange, S. *et al.* WFDE5 over land merged with ERA5 over the ocean (W5E5 v2.0). (2021) doi:10.48364/ISIMIP.342217.
63. Mölder, F. *et al.* Sustainable data analysis with Snakemake. *F1000Research* **10**, 33 (2021).
64. van Jaarsveld, B. GLOBGM_CMIP6: A Global Hyper-Resolution Groundwater Dataset for Assessing Historical and Future Groundwater Dynamics Under Climate and Socioeconomic Change - [globgm_historical_reference_gswp3-w5e5]. (2025) doi:10.24416/UU01-AKSHOX.
65. van Jaarsveld, B. GLOBGM_CMIP6: A Global Hyper-Resolution Groundwater Dataset for Assessing Historical and Future Groundwater Dynamics Under Climate and Socioeconomic Change - [ssp_rcp_monthly]. (2025) doi:10.24416/UU01-1BXLPD.

66. van Jaarsveld, B. GLOBGM_CMIP6: A Global Hyper-Resolution Groundwater Dataset for Assessing Historical and Future Groundwater Dynamics Under Climate and Socioeconomic Change - [ssp_rcp_average]. (2025) doi:10.24416/UU01-SLRFI7.
67. van Jaarsveld, B. GLOBGM_CMIP6: A Global Hyper-Resolution Groundwater Dataset for Assessing Historical and Future Groundwater Dynamics Under Climate and Socioeconomic Change - [quality_assurance]. (2025) doi:10.24416/UU01-16EJ3Y.
68. Reinecke, R. *et al.* Considerable gaps in our global knowledge of potential groundwater accessibility. (2023) doi:10.31223/X5SM0R.
69. Somers, L. D. & McKenzie, J. M. A review of groundwater in high mountain environments. *WIREs Water* **7**, e1475 (2020).
70. De Graaf, I. E. M., Gleeson, T., (Rens) Van Beek, L. P. H., Sutanudjaja, E. H. & Bierkens, M. F. P. Environmental flow limits to global groundwater pumping. *Nature* **574**, 90–94 (2019).
71. Gleeson, T. *et al.* GMD perspective: The quest to improve the evaluation of groundwater representation in continental- to global-scale models. *Geoscientific Model Development* **14**, 7545–7571 (2021).
72. Knoben, W. J. M., Freer, J. E. & Woods, R. A. Technical note: Inherent benchmark or not? Comparing Nash–Sutcliffe and Kling–Gupta efficiency scores. *Hydrology and Earth System Sciences* **23**, 4323–4331 (2019).
73. Gädeke, A. *et al.* Performance evaluation of global hydrological models in six large Pan-Arctic watersheds. *Climatic Change* **163**, 1329–1351 (2020).
74. Chen, Z. *et al.* World Karst Aquifer Map (WHYMAP WOKAM). (2017) doi:10.25928/B2.21_SFKQ-R406.
75. Gruber, S. Derivation and analysis of a high-resolution estimate of global permafrost zonation. *The Cryosphere* **6**, 221–233 (2012).
76. Ford, T. W. & Frauenfeld, O. W. Surface–Atmosphere Moisture Interactions in the Frozen Ground Regions of Eurasia. *Scientific Reports* **6**, 19163 (2016).

77. Diak, M. *et al.* Permafrost and groundwater interaction: current state and future perspective. *Frontiers in Earth Science* **11**, 1254309 (2023).

78. Cochand, M., Molson, J. & Lemieux, J. Groundwater hydrogeochemistry in permafrost regions. *Permafrost and Periglacial Processes* **30**, 90–103 (2019).